ISSN 1674-1056
http://cpb.iphy.ac.cn
http://iopscience.iop.org/cpb
中国物理 B
Chinese Physics
中国物理
Chinese Physics B

Photoelectrocatalytic oxidation of methane into methanol and formic acid over ZnO/graphene/polyaniline catalyst

Jia Liu(刘佳), Ying-Hua Zhang(张英华), Zhi-Ming Bai(白智明), Zhi-An Huang(黄志安), Yu-Kun Gao(高玉坤)

Citation: Chin. Phys. B . 2019, 28(4): 048101. **doi:** 10.1088/1674-1056/28/4/048101
Journal homepage: http://cpb.iphy.ac.cn; http://iopscience.iop.org/cpb

What follows is a list of articles you may be interested in

A review on MBE-grown HgCdSe infrared materials on GaSb (211)B substrates

Z K Zhang, W W Pan, J L Liu, W Lei
Chin. Phys. B . 2019, 28(1): 018103. **doi:** 10.1088/1674-1056/28/1/018103

Electrical and dielectric characterization of Au/ZnO/n—Si device depending frequency and voltage

I Orak, A Kocyigit, Ş Alındal
Chin. Phys. B . 2017, 26(2): 028102. **doi:** 10.1088/1674-1056/26/2/028102

Synthesis of graphene-supported monodisperse AuPd bimetallic nanoparticles for electrochemical oxidation of methanol

Xiao Hong-Jun, Shen Cheng-Min, Shi Xue-Zhao, Yang Su-Dong, Tian Yuan, Lin Shao-Xiong, Gao Hong-Jun
Chin. Phys. B . 2015, 24(7): 078109. **doi:** 10.1088/1674-1056/24/7/078109

Controllable synthesis, characterization, and growth mechanism of hollow $Zn_xCd_{1-x}S$ spheres generated by a one-step thermal evaporation method

Yang Zai-Xing, Zhong Wei, Au Chak-Tong, Du You-Wei
Chin. Phys. B . 2013, 22(10): 108101. **doi:** 10.1088/1674-1056/22/10/108101

Zn/O ratio and oxygen chemical state of nanocrystalline ZnO films grown at different temperatures

Fan Hai-Bo,Zheng Xin-Liang,Wu Si-Cheng,Liu Zhi-Gang,Yao He-Bao
Chin. Phys. B . 2012, 21(3): 038101. **doi:** 10.1088/1674-1056/21/3/038101

Photoelectrocatalytic oxidation of methane into methanol and formic acid over ZnO/graphene/polyaniline catalyst*

Jia Liu(刘佳), Ying-Hua Zhang(张英华), Zhi-Ming Bai(白智明)†, Zhi-An Huang(黄志安), and Yu-Kun Gao(高玉坤)

School of Civil and Resource Engineering, University of Science and Technology Beijing, Beijing 100083, *China*

(Received 16 October 2018; revised manuscript received 10 January 2019; published online 5 March 2019)

ZnO/graphene/polyaniline (PANI) composite is synthesized and used for photoelectrocatalytic oxidation of methane under simulated sun light illumination with ambient conditions. The photoelectrochemical (PEC) performance of pure ZnO, ZnO/graphene, ZnO/PANI, and ZnO/graphene/PANI photoanodes is investigated by cyclic voltammetry (CV), chronoamerometry (J–t) and electrochemical impedance spectroscopy (EIS). The yields of methane oxidation products, mainly methanol (CH_3OH) and formic acid (HCOOH), catalysed by the synthesized ZnO/graphene/PANI composite are 2.76 and 3.20 times those of pure ZnO, respectively. The mechanism of the photoelectrocatalytic process converting methane into methanol and formic acid is proposed on the basis of the experimental results. The enhanced photoelectrocatalytic activity of the ZnO/graphene/PANI composite can be attributed to the fact that graphene can efficiently transfer photo-generated electrons from the inner region to the surface reaction to form free radicals due to its superior electrical conductivity as an inter-media layer. Meanwhile, the introduction of PANI promotes solar energy harvesting by extending the visible light absorption and enhances charge separation efficiency due to its conducting polymer characteristics. In addition, the PANI can create a favorable π-conjunction structure together with graphene layers, which can achieve a more effective charge separation. This research demonstrates that the fabricated ZnO/graphene/PANI composite promises to implement the visible-light photoelectrocatalytic methane oxidation.

Keywords: methane conversion, photoelectrocatalysis, methanol, formic acid, ZnO NWAs, polyaniline

PACS: 81.05.Dz, 81.05.Fb, 81.05.ue, 81.07.–b **DOI:** 10.1088/1674-1056/28/4/048101

1. Introduction

Methane, as the principal constituent of natural gas, has long been considered to be a preferable energy alternative to traditional fossil fuels due to its high hydrogen-to-carbon ratio and lower CO_2 emissions. The global methane reserve is estimated to be approximately 1.4×10^{11} m^3.[1] However, the low energy density of methane compared with those of traditional fossil fuels restrains its on-board applicability, and makes transportation and storage difficult. It is also notable that methane is the second largest greenhouse gas that causes global warming as a result of the greenhouse effect.[2–4] Over the past two hundred years, thanks to the rapid changes in human production, a large amount of methane has been released into the atmosphere. The damaging effect of methane on the ozone layer is 20 times that of carbon dioxide. Therefore a mild method of catalytic conversion of methane into methanol and other oxygenates is of considerable practical value. In this way, the hydrocarbon of methane conversion may be used directly as fuel or may be converted into other oxygenated fuels and valuable products.

In earlier decades, much effort has been made to convert methane into fuels via thermo-catalysis.[5–7] However, the reaction process always requires high temperature or high pressure, which causes great energy consumption. Thus, other methods have been explored to achieve methane oxidation, such as electrocatalytic oxidation of methane. Until now, metal electrodes such as Pt, Au, Pd, and Ru, *etc*. have been investigated for methane oxidation and different products have been obtained such as CO and CO_2.[8–11] Nonetheless, these systems require either uneconomical noble metal or specific electrolyte (*e.g*., strong acid or alkaline). Being a mild reaction condition and environmentally friendly technique, photocatalysis is a viable technology for methane oxidation because it has shown promising utilization in many fields such as air purification and water splitting.[12–14] For example, WO_3, TiO_2, and NiO were reported as photocatalysts in methane oxidation process under the irradiation of ultra-violet (UV) or visible laser.[1,15–17] Ag decorated ZnO was also used as photocatalyst to oxidize methane under simulated sunlight illumination.[18] V-containing MCM-41 catalyst was synthesized and its photoactivity was evaluated for the selective photocatalytic oxidation of methane with NO under UV irradiation.[19] However, photocatalytic oxidation has several drawbacks, such as the high photoinduced charge recombination rate and low charge separation efficiency, which hinders the application of semiconductor photocatalysts. An attractive strategy to increase the photocatalytic efficiency is to apply an external bias potential to the anode coated by the photocatalyst, which is known

*Project supported by the National Natural Science Foundation of China (Grant Nos. 51602021 and 51474017) and the Fundamental Research Funds for the Central Universities (Grant No. FRF-TP-15-107A1).

†Corresponding author. E-mail: baizhiming2008@126.com

© 2019 Chinese Physical Society and IOP Publishing Ltd

as photoelectrocatalysis.[20–22]

One-dimensional ZnO nanomaterials are wide bandgap semiconductor materials with significant advantages in electrical transport, optics, optoelectronics, photocatalysis, field emission, electrochemistry, *etc*.[23–26] In addition, one-dimensional ZnO nanomaterials have high electron mobility, exceptional photoconductivity characteristics, large specific surface area, stable chemical properties, abundant sources, and low cost, which makes them an ideal material for preparing the photoelectrocatalysis.[27,28] However, the low utilization rate of visible light due to its wide bandgap and high recombination rate of photogenerated carriers limits the application of ZnO in the field of photocatalysis. Therefore, many studies have been attempted to improve the photocatalytic activity of ZnO, such as doping,[29–31] deposition of quantum dots,[32,33] and construction of heterojunctions with other semiconductors.[34,35] In particular, coupling ZnO with carbon nanomaterials, such as graphene to form a carbon–ZnO photocatalyst, has proven to effectively promote the photocatalytic efficiency. The extremely high electron mobility and large specific surface area of graphene enables it to act as an electron mediator to inhibit photoinduced charge carriers from being recombined.[36–38]

The process of photoelectrocatalytic oxidation can enhance the quantum efficiency by introducing an external bias potential. With regard to this process, on the one hand, PANI is one of the conducting polymers with the delocalized conjugated structure, and its benzenoid and quinonoid units with several redox states make it a promising candidate in electrocatalysis.[39,40] On the other hand, the PANI has high charge carrier mobility and visible-light absorption efficiency, making it an ideal supplier for electron donors and hole transporters upon visible light excitation in photocatalytic process.[41,42]

So far, there has been little research on methane oxidation via photoelectrocatalysis. In the present work, for the first time methane is converted into methanol and formic acid via photoelectocatalysis under simulated sun light illumination in ambient conditions. First, we synthesize ZnO NWAs, ZnO/graphene, ZnO/PANI and ZnO/graphene/PANI composites and characterize the morphostructures, crystalline phases and absorption spectra of the samples. Then, their PEC properties are investigated under simulated sunlight illumination by recording the CV, *J*–*t*, and EIS curves. The as-prepared ZnO/graphene/PANI nanocatalyst shows a remarkable photocatalytic activity for visible light photoelectrocatalytic methane oxidation. The enhanced performance is attributed to the fact that the introduction of graphene and PANI extends the visible light absorption with enhanced solar energy harvesting and increases the separation efficiency of photo-induced charge carriers by inhibiting the electron–hole pairs from being recombined, thus resulting in an increase in the number of holes that participated in the photooxidation process. This research demonstrates that the fabricated ZnO/graphene/PANI composite greatly promises to implement the simulated sun light photoelectrocatalytic methane oxidation. Furthermore, it contributes to a better understanding of the mechanism of the photoelectrocatalytic process converting methane into methanol and formic acid, which brings new ideas to the direct oxidation and utilization of methane.

2. Experiment

2.1. Fabrication of ZnO NWAs

The ZnO NWAs were prepared by the hydrothermal method.[43] First, the FTO glasses (1 cm×1.5 cm) were cleaned by ultrasonication in acetone, ethanol and deionized water, sequentially for 10 min. Then, the colloidal seed solution (0.25-mM $Zn(CH_3COO)_2{\cdot}2H_2O$ solution) was spin-coated onto an FTO substrate. After being dried naturally, the FTO glasses were annealed for 30 min at 350 °C. Then they were placed into a polytetrafluoroethylene autoclave containing 150 ml of zinc nitrate hydrate $[Zn(NO_3)_2{\cdot}6H_2O]$ (25 mM) and hexamethylenetetramine $[(CH_2)_6N_4]$ (25 mM) aqueous solution and were kept at 95 °C for 8 h. Finally, the glasses were cleaned with deionized water carefully to remove the residual surface salts.

2.2. Synthesis of ZnO/graphene/PANI catalyst

Figure 1 shows the synthetic procedure and illustrates the composition of the as-prepared ZnO/graphene/PANI composite. 1-mg·mL^{-1} graphene aqueous solution (Plannano Energy Technologies Ltd., Tianjin) was first spin-coated onto ZnO NWAs attached on the FTO substrate at a low speed of 600 rpm·min^{-1}, followed by a high speed of 2000 rpm·min^{-1}.

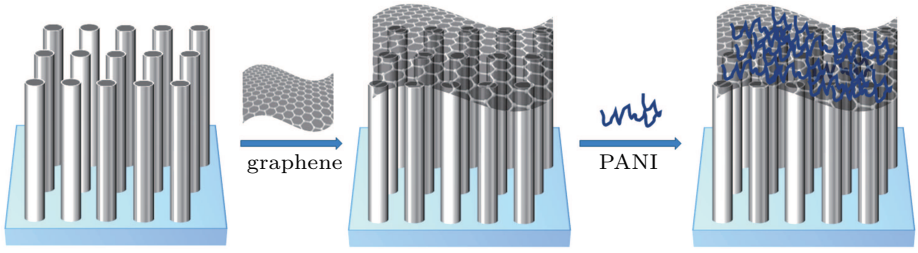


Fig. 1. Stepwise synthetic procedure and structure of ZnO/graphene/PANI composite.

This coating process was repeated three times to obtain the graphene thin film. The PANI (Macklin Ltd., Shanghai) was dispersed in ethanol to form a 10-mg·ml^{-1} stable suspension. Then PANI suspension was deposited on the top of graphene following the process described above. To conduct comparative experiments, the graphene and PANI were spin-coated onto the ZnO NWAs respectively to synthesize ZnO/graphene and ZnO/PANI photoanodes.

2.3. Characterization of materials

We acquired scanning electron microscopy (SEM) images with a SUPRA55 field-emission scanning electron microscope (FESEM). A Rigaku DMAX-RB x-ray diffractometer, equipped with a Cu Kα x-ray radiation source, was used to examine the x-ray diffraction patterns (XRD) of the samples. Fourier-transform infrared spectra (FT-IR) of the samples are recorded on an Excalibur 3100 spectrometer in a range of 400 cm^{-1}–4000 cm^{-1}. A Cary 5000 UV-vis-NIR spectrophotometer was used to obtain the absorption spectra of the samples over a range of 200 nm–800 nm.

2.4. Photoelectrocatalytic experiments

The photoelectrocatalytic oxidation of methane was conducted in a glass electrolytic cell with a 180-ml capacity. Inside the electrolytic cell, a three-electrode system, connected with an electrochemical workstation (CHI 660E, CH Instruments Inc., USA), was used to investigate the PEC properties of ZnO, ZnO/graphene, ZnO/PANI and ZnO/graphene/PANI photoanodes. The three-electrode system contained a saturated Ag/AgCl reference electrode (0.197 V), a Pt counter electrode and a working electrode. The working electrode was FTO glasses coated with ZnO, ZnO/Graphene, ZnO/PANI or ZnO/Graphene/PANI and, sealed by polyacrylate glue to cover the edges and backside. The electrolytic cell was filled with 130-ml Na_2SO_4 aqueous solution (0.05 M). The photoelectrocatalytic experiments were carried out at room temperature and atmospheric pressure. In a typical reaction batch: after the three-electrode system and electrolyte were prepared ready, argon was injected into the electrolytic cell through the gas intake tube at a flow rate of 50 ml·min^{-1} for 15 min to purge the solution. Then, the PEC properties were investigated by an electrochemical workstation and the CV, *J*–*t*, and EIS curves were recorded under the dark and illumination conditions. As for the illumination condition, a 300-W Xe lamp (PLSSXE300, Perfect-Light Co., China) equipped with an AM 1.5-G filter was used to provide simulated sunlight illumination from the front side of the samples. The light intensity was calibrated to be 100 mW·cm^{-2}. After the PEC properties were recorded, the solution was saturated with methane (99.995%, BAPB Co., China) at a flow rate of 50 ml·min^{-1} for 15 min. Then the PEC characterization process was adopted as described above. In addition, liquid samples were extracted from the cell by a syringe at regular intervals (30 min) for the following characterization of reaction products by using a gas chromatograph (SHIMADZU GC-2014) equipped with a Restek rtx-5 column, a flame ionization detector and a thermal conductivity detector.

3. Results and discussion

Figure 2(a) shows a top-view SEM image of the ZnO NWAs. As can be seen, the ZnO NWAs are vertically aligned on the FTO substrate, and the hexagonal nanowires have a smooth surface. The average diameter and length of the nanowires are approximately 100 nm and 2.5 μm, respectively. Figure 2(b) depicts the top-view SEM image of ZnO/graphene composite. It can be seen from Fig. 2(b) that the crumpled silk-like graphene sheets attach to the top of the ZnO nanowires and the transparent feature indicates that the graphene sheet is ultrathin. The morphology of sample (Fig. 2(c)) shows the coexistence of floccules and the nanorod structure, demonstrating the imbedding of PANI in the ZnO NWAs. It can be seen clearly that the flocculated PANI is evenly packed into the voids of ZnO nanorods, which will contribute to the formation of p–n junction between ZnO and PANI. As can be seen in Fig. 2(d), the flocculent PANI agglomerates into petal-like nanofibers, which clearly spread over the surface of graphene nanosheets.

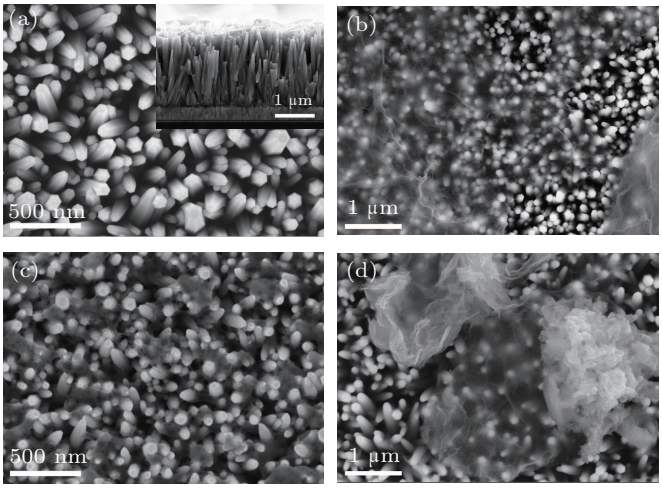


Fig. 2. Top view SEM image of (a) pristine ZnO NWAs, (b) ZnO/graphene, (c) ZnO/PANI, and (d) ZnO/graphene/PANI composite. The inset shows cross-sectional view of ZnO NWAs.

Figure 3 shows the XRD pattern of the ZnO NWAs, ZnO/graphene, ZnO/PANI and ZnO/graphene/PANI composite. For each of them, peak at 31.8°, 34.4°, 56.6°, 72.5°, and 76.9° can be obviously observed, which correspond to (100), (002), (110), (004), and (202) crystal planes of hexagonal ZnO (JCPDS NO.36-1451).[44] The sharp (002) peak indicates that the ZnO nanowires are highly *c*-axis oriented. However, none

of the diffraction peaks related to graphene and PANI are observed in the other three samples, suggesting that the graphene and PANI are amorphous in the composite and the introduction of graphene and PANI has no effect on the crystal structure of the ZnO NWAs.

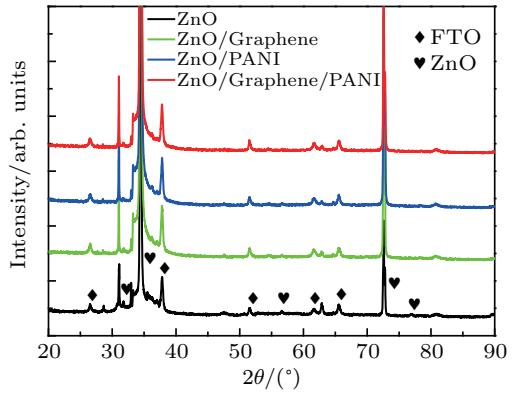


Fig. 3. XRD pattern of ZnO NWAs, ZnO/graphene, ZnO/PANI, and ZnO/graphene/PANI composite on FTO substrate.

Figure 4(a) depicts the ultra-violet-visible (UV-vis) absorption spectrum of ZnO NWAs, ZnO/graphene, ZnO/PANI, and ZnO/graphene/PANI composites on the FTO substrate. For the pure ZnO NWAs, exceptional absorption can be observed in the ultraviolet region (< 400 nm) due to the wide band gap of ZnO. After graphene is introduced, an enhancement of absorption in both the UV and visible region can be observed. For the PANI modified composites, the peak appears at approximately 440 nm corresponding to the band gap of PANI (2.8 eV), indicating that PANI is successfully modified on ZnO NWAs. Compared with the absorption of neat ZnO, the absorption of ZnO/PANI increases over the entire range of 200 nm–800 nm. Among them, the ZnO/graphene/PANI composite shows the most exceptional enhancement, which indicates that our hybridization is effective to extend the absorption of ZnO to the visible light range. The obvious improvement of the utilization of solar energy may be attributed to the p–p* transition of the benzenoid ring, polaron–p*, and p–polaron exaction transition of the quinonoid rings in the PANI structure, thus leading to a high absorption both in the UV region and the visible-light region.[45]

Figure 4(b) shows the Fourier transform infrared spectroscopy (FTIR) spectrum of pure ZnO, graphene, PANI and ZnO/graphene, ZnO/PANI, ZnO/graphene/PANI composites. For pure graphene, the presence of different functionalities can be found at 1566 cm^{-1} and 1180 cm^{-1}, corresponding to C=C skeletal vibration and C–OH stretching vibration. The peaks also appear in the spectrum of ZnO/graphene composite, shifting to lower wavenumbers of 1558 cm^{-1} and 1177 cm^{-1}, indicating that the graphene is successfully modified into ZnO NWAs and a chemical interaction is generated between graphene and ZnO. In the spectrum of bare PANI, the characteristic absorption peaks appear at 1549cm^{-1}, 1439 cm^{-1}, 1285 cm^{-1}, 1021 cm^{-1}, and 793cm^{-1} corresponding to the C=C stretching mode of quinoid ring, the C=C stretching mode of the benzenoid ring, the stretching mode of C–N, the stretching mode of N=Q=N, where Q represents the quinoid ring, and the C–H bonding mode of aromatic rings.[46] The ZnO/PANI composite also shows the same characteristic peaks. However, compared with the corresponding peaks of pure PANI shown above, the peaks of ZnO/PANI composite shift to higher wavenumbers of 1554 cm^{-1}, 1441 cm^{-1}, 1287 cm^{-1}, 1024 cm^{-1}, and 797 cm^{-1}. The shift may be ascribed to the formation of hydrogen bonding between ZnO and the NH groups of PANI on the surface of the ZnO NWAs. The ZnO/graphene/PANI composite shows a similar spectrum to that of PANI, it also contains the functional groups of graphene.

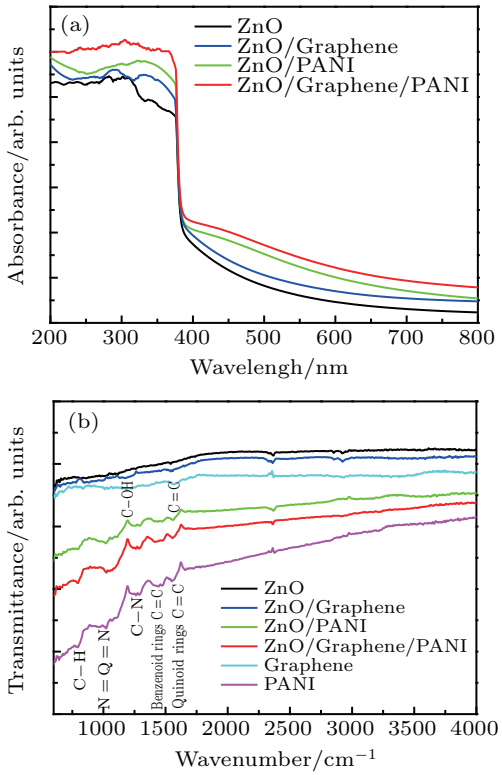


Fig. 4. (a) UV-vis absorption spectrum of ZnO NWAs, ZnO/graphene, ZnO/PANI, and ZnO/graphene/PANI composites on FTO substrate. (b) FTIR spectrum of pure ZnO, graphene, PANI, and ZnO/graphene, ZnO/PANI, ZnO/graphene/PANI composites.

Cyclic voltammograms are recorded in the dark and under illumination to explore the reactions that occur throughout the entire potential window. As can be seen in Fig. 5(a), the hydrogen adsorption–desorption peaks of the CV curves saturated with methane are partially suppressed compared with the argon purged ones, indicating the presence of an adsorbed species covering the electrode surface.[47,48] After the hydrogen region, the current begins to increase and an obvious oxidation peak located at 0.51 V can be observed in the anodic

scan. This can be presumably attributed to the methane oxidation process, where the CH_4 absorbed on the electrode reacts with ·OH to form a $\cdot CH_3$ intermediate and then generates a C_1 oxygenated hydrocarbon species.[48,49] According to the GC result, the main oxidation products are methanol and formic acid. It can also be observed that the current densities of the CV curves under illumination are much higher those in the dark throughout nearly the entire potential window, whether in the absence or presence of CH_4, revealing that the simulated sunlight illumination greatly enhances the catalytic activity of ZnO electrode and further proves that ZnO exhibits exceptional activity for photoelectrocatalytic methane oxidation. Two main properties contribute to its great exhibition. First, the valence band maximum of ZnO is lower than the potential of $\cdot OH/OH^-$ (+2.59 V *versus* NHE),[50,51] and the conduction band minimum is higher than the potential of O_2/O_2^- (−0.16 V *versus* NHE),[52] which makes it possible to generate O_2^- and ·OH radicals and further induce the methane oxidation to occur. Second, the rich defective surfaces of ZnO NWAs make it easier for the surface reactions to occur and keep on going. In addition, the pores and channels of ZnO NWAs significantly reduce the liquid sealing effect.[53]

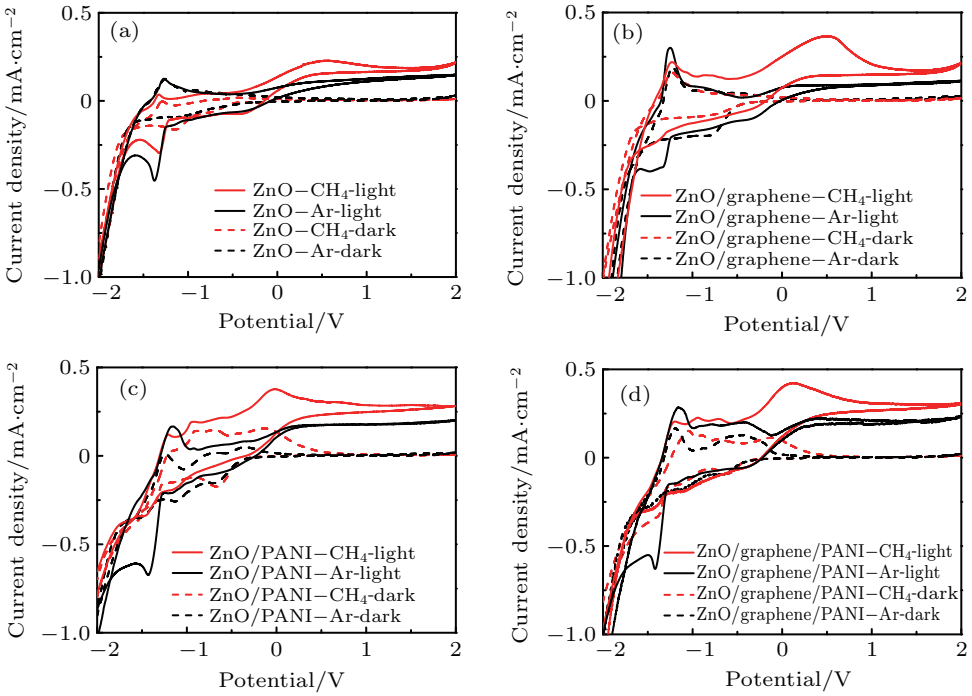


Fig. 5. Cyclic voltammogram recorded on (a) ZnO, (b) ZnO/graphene, (c) ZnO/PANI, (d) ZnO/graphene/PANI electrodes saturated with argon and methane in the dark and under illumination at a scan rate of 0.1 V·s^{-1} (*versus* Ag/AgCl).

Figure 5(b) shows the cyclic voltammogram of ZnO/graphene electrode. Compared with the CV curves of bare ZnO, the CV curves of ZnO/graphene saturated with argon exhibit an alleviated hydrogen adsorption peak and an elevated desorption peak. In addition, a pair of redox can be observed at approximately −0.85 V, which may be attributed to the redox reaction of OH^- or H^+ with the residual functional groups in the matrix of graphene.[54] In the CV curve after bubbling methane, the ZnO/graphene electrode shows a much higher oxidation peak current and lower on-set potential and peak potential compared with pure ZnO. This implies that the ZnO/graphene has enhanced electrocatalytic activity for methane oxidation, which can be attributed to the delocalized conjugated structure and superior electrical conductivity of graphene, thus making the photo-generated electrons more efficiently transfer and the e^-/h^+ pairs inhibit from being recombined.[37]

In Fig. 5(c), three pairs of redox peaks can be observed in the CV curve purged with argon. They are assigned to the interconversion between the different oxidation states (leucoemeraldine, pernigraniline and emeraldine) of PANI.[55] The improvement of the peak current and more negative on-set potential of methane oxidation indicate that the ZnO/PANI is a better electrocatalyst, owing to the high conductivity of PANI and the mixed-conducting nature of PANI-coated ZnO which enhances electron and proton transport within the electrode.

Figure 5(d) shows the CV of a ZnO/graphene/PANI electrode in the absence and presence of CH_4 in the dark and under illumination. The shapes of the curves are similar to those of the ZnO/PANI electrode; however, it exhibits the highest peak current of 0.43 mA·cm^{-2}, which is 1.87 times that of bare ZnO (0.23 mA·cm^{-2}) and the most negative on-set potential of −0.57 V. The comparison in Table 1 reveals that ZnO/graphene/PANI composite exhibits the best performance for photoelectrocatalytic methane oxidation. The enhancement can be ascribed to the integration of graphene and PANI on ZnO NWAs. They both play an

important role in the improvement thanks to their individual characteristics, as described above. Moreover, the PANI can create a favorable π-conjunction structure together with graphene layers, which can achieve a more effective charge separation.[56]

Table 1. Comparison among electrocatalytic activities of methane oxidation on ZnO, ZnO/graphene, ZnO/PANI, and ZnO/graphene/PANI.

Electrode	On-set potential/V	Peak potential/V	Peak current/mA·cm^{-2}
ZnO	–0.42	0.51	0.23
ZnO/graphene	–0.49	0.49	0.36
ZnO/PANI	–0.52	–0.03	0.38
ZnO/graphene/PANI	–0.57	0.10	0.43

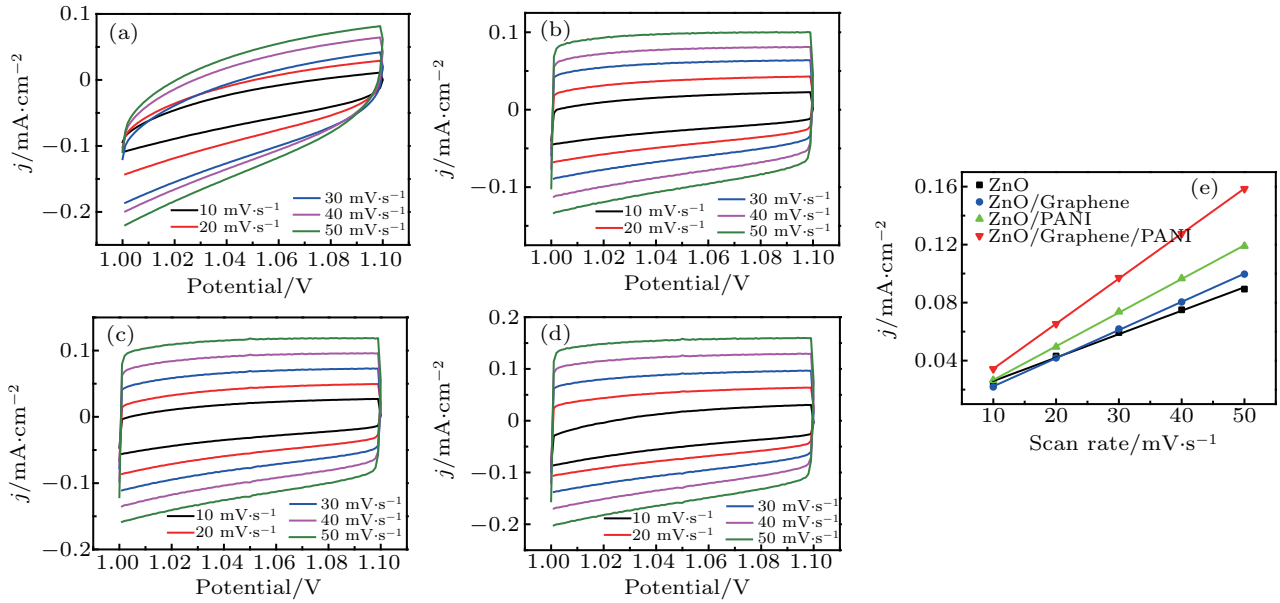


Fig. 6. Electrochemical double layer capacitance curves on (a) ZnO, (b) ZnO/graphene, (c) ZnO/PANI, (d) ZnO/graphene/PANI with scan rates ranging from 10 mV·s^{-1} to 50 mV·s^{-1} (*versus* Ag/AgCl) in 1-M Na_2SO_4.

The electrochemistry activity of an electrocatalyst is determined by its intrinsic activity and the number of active sites.[57] Thus, the electrocatalytically active surface area (ECSA) is estimated to reveal the electrochemistry activity of the as-prepared electrodes. The double-layer capacitance (C_{dl}), which is generally proportional to the ECSA,[58] is investigated by using cyclic voltammetry (CV) as shown in Figs. 6(a)–6(d). Half of each difference between the positive and negative current density in the center part of the scanning potential ranges is plotted *versus* the voltage scan rate in Fig. 6(e), in which each of the slopes is the electrochemical double-layer capacitance. The C_{dl} value of ZnO, ZnO/graphene, ZnO/PANI and ZnO/graphene/PANI are 1.62, 1.94, 2.32, and 3.11 mF·cm^{-2}, respectively. As can be seen, the ZnO/graphene/PANI displays the highest ECSA, the enhancement in the activity of ZnO/graphene/PANI is most likely associated with its high intrinsic activity deriving from the surface modification.[59] In addition, the excellent electrical conductivity of graphene and PANI support facilitate the charge transfer in the hybrid.

Figure 7(a) shows the transient current density with 10-s light on/off cycles for the samples at 1 V (*versus* Ag/AgCl). The four samples all show instantaneous photoresponses to the switching irradiation, implying a reasonable photoelectrocatalytic process at the modified electrodes. Among them, the ZnO/graphene/PANI composite exhibits the most significant photoresponse, whose photocurrent under illumination reaches up to 0.30 mA·cm^{-2}, approximately 1.7 times that of 0.18 mA·cm^{-2} for ZnO NWAs, indicating that it possesses the highest photoelectrocatalytic methane oxidation efficiency in all of the electrodes. The ZnO/graphene and ZnO/PANI composites also show that their photocurrent values are improved up to approximately 0.20 mA·cm^{-2} and 0.23 mA·cm^{-2}. The charge transfer properties of the four samples are analyzed by using EIS plots acquired under dark and light conditions. The radius of Nyquist curve represents the charge transfer resistance. As shown in Fig. 6(b), in either the absence or presence of illumination, ZnO/graphene/PANI has a smaller curve radius than the others, suggesting that a more effective separation rate of photogenerated electron–hole pairs and a faster interfacial charge transfer occurring on ZnO/graphene/PANI composite. For the same photoanode, the curve radius under illumination is much smaller than that under dark conditions, revealing that the simulated sunlight can enhance the inter-

face charge transport process. In conclusion, the PEC results strongly prove that the ternary ZnO/graphene/PANI hybrid can substantially inhibit the electron–hole recombination and improve the electron transfer rate, therefore efficiently enhancing the photoelectrocatalytic performance.

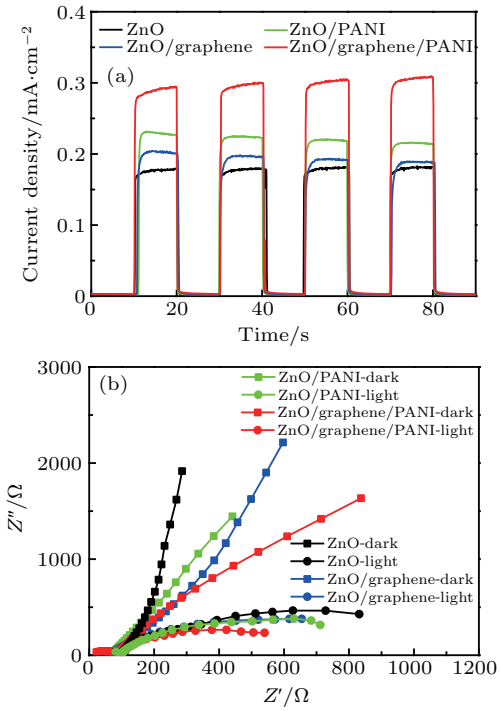


Fig. 7. (a) Chronoamperometric *J*–*t* curve collected at 1 V (*versus* Ag/AgCl) for ZnO NWAs, ZnO/graphene, ZnO/PANI, and ZnO/graphene/PANI composites under chopped illumination conditions. (b) EIS plot of ZnO NWAs, ZnO/graphene, ZnO/PANI, and ZnO/graphene/PANI composites in the dark and under light illumination.

Figure 8 shows the yields of the major products (CH_3OH and HCOOH) obtained after 2.5-h illumination. Comparing with pure ZnO NWAs, the modification with graphene or PANI increases the yield of products. Of them, the ZnO/graphene/PANI composite exhibits the most significant enhancement of the yield of methanol (CH_3OH) and formic acid (HCOOH), with the yields when catalyzed by the synthesized ZnO/graphene/PANI composite being 2.76 and 3.20 times those of pure ZnO photocatalyst, respectively. This can be attributed to the fact that the introduction of graphene and PANI can expedite the separation of electron–hole pairs, which favors the production of hydroxyl radicals and in turn stimulate the production of methanol and formic acid.

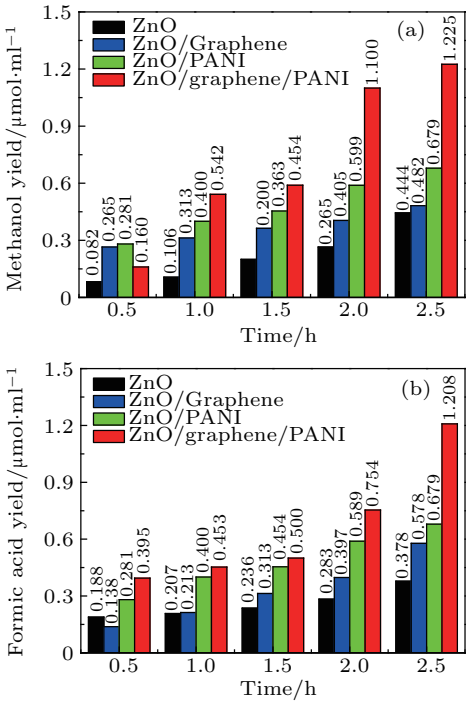


Fig. 8. Yields of (a) CH_3OH and (b) HCOOH in the photoelectrocatalytic oxidation of CH_4 with catalyst of ZnO NWAs, ZnO/graphene, ZnO/PANI, and ZnO/graphene/PANI composites under simulated sunlight illumination. Data correspond to 2.5-h illumination in a continuous methane flow of 50 mL·min^{-1}.

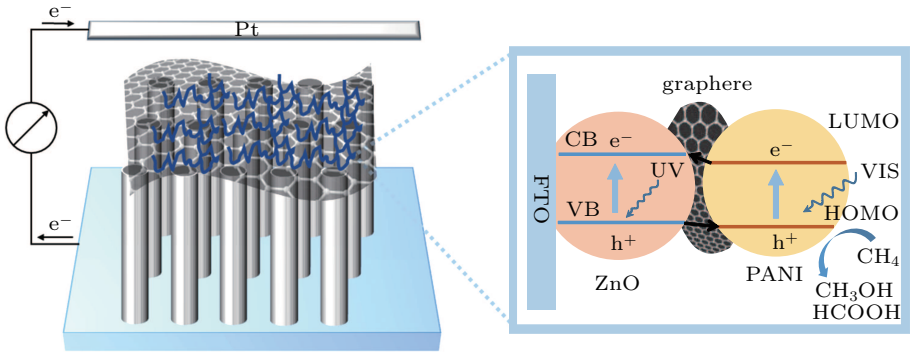


Fig. 9. Mechanism of ZnO/graphene/PANI composite to enhance photocatalytic activity under simulated sunlight.

Based on the data that we have obtained, the mechanism of enhancing the photoelectrocatalytic performance for the as-prepared ZnO/graphene/PANI composite is proposed; as shown in Fig. 9. Under simulated sunlight illumination, electrons in the valence bands (VB) of ZnO can be excited to their conduction bands (CB). Moreover, the introduction of PANI extends the visible light absorption, and thus, more electron–hole pairs can be generated in PANI. The electrons in LUMO of PANI can easily transfer to CB of ZnO due to the π-conjunction structure between PANI and graphene, thus resulting in efficient charge separation and therefore inhibiting the recombination process. Simultaneously, the holes left on

the VB of ZnO will flow to the HOMO of PANI via graphene medium layer, triggering the formation of reactive hydroxyl radical OH·, which is responsible for the oxidation of methane.

The reaction shown below illustrates the electron transfer process of methane oxidation. As depicted above, with simulated sunlight illumination, ZnO/graphene/PANI composite will generate e^-/h^+ pairs. The positive hole h^+_{vb} will then be occupied with water splitting, forming a hydroxyl radical and a proton. Meanwhile, the e^-_{cb} reacts with the proton to create an H· radical, which further generates hydrogen. Finally, the aforementioned hydroxyl radicals will react with methane to produce methyl radicals, which will further react with an additional water molecule, forming methanol and hydrogen. The methanol can then interact with the OH· radical to produce formic acid[15,17,60,61] in the following sequence:

$$
\begin{aligned}
&\mathrm{ZnO/graphene/PANI} \xrightarrow{h\nu} \mathrm{e^- + h^+},\\
&\mathrm{h^+ + H_2O \rightarrow H^+ + \cdot OH},\\
&\mathrm{e^- + H^+ \rightarrow H\cdot},\\
&\mathrm{H\cdot + H\cdot \rightarrow H_2},\\
&\mathrm{CH_4 + \cdot OH \rightarrow \cdot CH_3 + H_2O},\\
&\mathrm{\cdot CH_3 + H_2O \rightarrow CH_3OH + \frac{1}{2}H_2},\\
&\mathrm{CH_3OH + \cdot OH \rightarrow HCOOH + H_2 + H\cdot}.
\end{aligned}
$$

4. Conclusions and perspectives

In the present research, we report the fabrication of ZnO/graphene/PANI composite and its application as photoanode in methane oxidation. The CV curves reveal the behavior and intensity of the oxidation and reduction reactions in the entire process of methane oxidation. Moreover, the *J*–*t* and EIS curves indicate that the ZnO/graphene/PANI photoanode exhibits an enhanced photoelectrocatalytic activity under simulated sunlight illumination. The improved performance is attributed to the following crucial factors: (i) as an inter-medium layer, graphene has an exceptional ability to transfer photo-generated electrons, and thus, the photo-generated electrons in the synthesized photocatalyst can easily migrate from the inner region to the surface to participate in the surface reaction to form free radicals; (ii) the introduction of PANI extends the visible light absorption with enhanced solar energy harvesting, and promotes the electron transfer rate and the charge separation efficiency; and (iii) the PANI can create a favorable π-conjunction structure together with graphene layers, which can achieve a more effective charge separation. The research reported here shows the great potential for ZnO/graphene/PANI to serve as a photoelectrocatalyst in methane oxidation.

References

[1] Crabtree R H 1995 *Chem. Rev.* **95** 987
[2] Cao M K, Gregson K and Marshall S 1998 *Atmos. Environ.* **32** 3293
[3] Ruppel C D 2011 *Nat. Educ. Knowl.* **3** 29
[4] Howarth R W, Santoro R and Ingraffea A 2011 *Climatic Change* **106** 679
[5] Hammond C, Forde M M, Rahim A, Hasbi M, Thetford A, He Q, Jenkins R L, Dimitratos N, Lopez-Sanchez J A and Dummer N F 2012 *Angew. Chem. Int. Ed.* **51** 5129
[6] Zhang Q J, He D H and Zhu Q M 2008 *J. Nat. Gas Chem.* **17** 24
[7] Alvarez-Galvan M C, Mota N, Ojeda M, Rojas S, Navarro R M and Fierro J L G 2011 *Catal. Today* **171** 15
[8] Sustersic M G, Córdova O R, Triaca W E and Arvía A J 1980 *J. Electrochem. Soc.* **127** 1242
[9] Qiao J, Tang S N, Tian Y N, Shuang S M, Dong C and Choi M M F 2009 *Sens. Actuators B: Chem.* **138** 402
[10] Jafarian M, Mahjani M G, Heli H, Gobal F and Heydarpoor M 2003 *Electrochem. Commun.* **5** 184
[11] Joglekar M, Nguyen V, Pylypenko S, Ngo C, Li Q, O'Reilly M E, Gray T S, Hubbard W A, Gunnoe T B, Herring A M and Trewyn B G 2016 *J. Am. Chem. Soc.* **138** 116
[12] Dong F, Ou M Y, Jiang Y K, Guo S and Wu Z B 2014 *Ind. & Eng. Chem. Res.* **53** 2318
[13] Nischk M, Mazierski P, Gazda M and Zaleska A 2014 *Appl. Catal. B: Environ.* **144** 674
[14] Naldoni A, Bianchi C L, Pirola C and Suslick K S 2013 *Ultrason. Sonochem.* **20** 445
[15] Hameed A, Ismail I M I, Aslam M and Gondal M A 2014 *Appl. Catal. A: Gen.* **470** 327
[16] Gondal M A, Hameed A and Suwaiyan A 2003 *Appl. Catal. A: Gen.* **243** 165
[17] Gondal M A, Hameed A, Yamani Z H and Arfaj A 2004 *Chem. Phys. Lett.* **392** 372
[18] Chen X X, Li Y P, Pan X Y, Cortie D, Huang X T and Yi Z G 2016 *Nat Commun.* **7** 12273
[19] Hu Y, Nagai Y, Rahmawaty D, Wei C H and Anpo M 2008 *Catal. Lett.* **124** 80
[20] Wahl A, Ulmann M, Carroy A, Jermann B, Dolata M, Kedzierzawski P, Chatelain C, Monnier A and Augustynski J 1995 *J. Electroanal. Chem.* **396** 41
[21] Georgieva J, Valova E, Armyanov S, Philippidis N, Poulios I and Sotiropoulos S 2012 *J. Hazard. Mater.* **211–212** 30
[22] Fraga L E, Anderson M A, Beatriz M L P M A, Paschoal F M M, Romão L P and Zanoni M V B 2009 *Electrochim. Acta* **54** 2069
[23] Orak I, Kocyigit A and Alındal S 2017 *Chin. Phys. B* **26** 028102
[24] Yang T Y, Kong C Y, Ruan H B, Qin G P, Li W J, Liang W W, Meng X D, Zhao Y H, Fang L and Cui Y T 2012 *Acta Phys. Sin.* **61** 168101 (in Chinese)
[25] Jin Y P, Zhang B, Wang J Z and Shi L Q 2016 *Chin. Phys. Lett.* **33** 058101
[26] Yang X Y, Cheng J Y, Li B, Cao W Q, Yuan J, Zhang D Q and Cao M S 2012 *Chin. Phys. Lett.* **29** 108101
[27] Wang Y J, Shi R, Lin J and Zhu Y F 2011 *Energy & Environ. Sci.* **4** 2922
[28] Bai X J, Wang L, Zong R L, Lv Y H, Sun Y Q and Zhu Y F 2013 *Langmuir Acs J. Surf. & Colloids* **29** 3097
[29] Wu Y N, Wu D C, Dong C J, Zhang P P, Ji H X and He L 2011 *Acta Phys. Sin.* **60** 77505 (in Chinese)
[30] Zhong W W, L F M, Cai L G, Ding P, Liu X Q and Li Y 2011 *Acta Phys. Sin.* **60** 118102 (in Chinese)
[31] Wu Z H and Duan W Q 2012 *Acta Phys. Sin.* **61** 137502 (in Chinese)
[32] Chen H M, Chen C K, Chang Y C, Tsai C W, Liu R S, Hu S F, Chang W S and Chen K H 2010 *Angew. Chem.* **122** 6102
[33] Wang G, Yang X, Qian F, Zhang J Z and Li Y 2010 *Nano Lett.* **10** 1088
[34] Shao M F, Ning F Y, Wei M, Evans D G and Xue D 2014 *Adv. Funct. Mater.* **24** 580
[35] Singh N S, Kumar L, Kumar A, Vaisakh S, Singh S D, Sisodiya K, Srivastava S, Kansal M, Rawat S, Singh T A, Tanya and Anita 2017 *Mater. Sci. Semicond. Process.* **60** 29
[36] Bai Z M, Yan X Q, Kang Z, Hu Y P, Zhang X H and Zhang Y 2015 *Nano Energy* **14** 392
[37] Xu T G, Zhang L W, Cheng H Y and Zhu Y F 2011 *Appl. Catal. B Environ.* **101** 382
[38] Fu C, He D W, Wang Y S, Fu M, Geng X and Zhuo Z L 2015 *Chin. Phys. B* **24** 87801
[39] Zhang L L, Huang D, Hu N T, Yang C, Li M, Wei H, Yang Z, Su Y J and Zhang Y F 2017 *J. Power Sources* **342** 1

[40] Fan S N, Liu R W, Ma R S, Yu S S, Li M, Zheng W T and Hu S X 2017 *Chin. Phys. B* **26** 048102
[41] Nsib M F, Saafi S, Rayes A, Moussa N and Houas A 2016 *J. Energy Inst.* **89** 694
[42] Anjum M, Oves M, Kumar R and Barakat M A 2017 *Int. Biodeterioration & Biodegradation* **119** 66
[43] Li Z H, Feng S L, Liu S Y, Li X, Wang L and Lu W Q 2015 *Nanoscale* **7** 19178
[44] Weng B, Yang M Q, Zhang N and Xu Y J 2014 *J. Mater. Chem. A* **2** 9380
[45] Jing L, Yang Z Y, Zhao Y F, Zhang Y X, Guo X, Yan Y M and Sun K N 2014 *J. Mater. Chem. A* **2** 1068
[46] Singh J, Bhondekar A P, Singla M L and Sharma A 2013 *ACS Appl. Mater. & Interfaces* **5** 5346
[47] Gasteiger H A, Markovic N, Jr P N R and Cairns E J 1994 *J. Phys. Chem.* **9746** 326
[48] Hahn F and Melendres C A 2001 *Electrochim. Acta* **46** 3525
[49] Sustersic M G 1980 *J. Electrochem. Soc.* **127** 1242
[50] Koppenol W H and Liebman J F 1984 *J. Phys. Chem.* **88** 99
[51] Chen X X, Huang X T and Yi Z G 2014 *Chemistry* **20** 17590
[52] Wood P M 1988 *Biochem. J.* **253** 287
[53] Xu C W, Cheng L Q, Shen P K and Liu Y L 2007 *Electrochem. Commun.* **9** 997
[54] Chen S, Zhu J W and Wang X 2010 *J. Phys. Chem. C* **114** 11829
[55] Sawangphruk M and Kaewsongpol T 2012 *Mater. Lett.* **87** 142
[56] Tang Y H, Wu N, Luo S L, Liu C B, Wang K and Chen L Y 2012 *Macromol. Rapid Commun.* **33** 1780
[57] Seh Z W, Kibsgaard J, Dickens C F, Chorkendorff I, Nørskov J K and Jaramillo T F 2017 *Science* **355** eaad4998
[58] Wang Z Q, Liu Z A, Du G, Asiri A M, Wang L, Li X N, Wang H J, Sun X P, Chen L and Zhang Q J 2018 *Chem. Commun.* **54** 7
[59] Zhang H B, Yu L, Chen T, Zhou W and Lou X W 2018 *Adv. Funct. Mater.* 201807086
[60] Yuliati L and Yoshida H 2008 *Chem. Soc. Rev.* **37** 1592
[61] Taylor C and Noceti R 2000 *Catal. Today* **55** 259